

NUMERICAL IMPLEMENTATION OF SURFACE CATALYSIS, REACTION, AND SUBLIMATION

Chul Park

Department of Aerospace Engineering, Korea Advanced Institute of Science and Technology
373-1 Guseong-dong, Yuseong-gu, Daejeon, 305-701 SOUTH KOREA

cpark216@kaist.ac.kr

ABSTRACT

This lecture consists of three parts: 1) quantification of rates of gas-surface interaction, 2) formulation of gas-surface balance conditions, and 3) survey of the gas-surface interaction problems in the entry flights of various planets. The first part reviews the role of surface rates and flow parameters in Goulard's theory, the catalytic rates for Martian entry problem, the reaction rates for oxidation and nitridation of carbon, rough surfaces, and the relationship between forward and reverse surface rates. The second part covers the method of expressing the diffusion flux at wall, derivation of the mass balance condition at wall, and its implementation in the boundary layer and computational-fluid-dynamics formulations. In the third part, a brief survey is made of the gas-surface interaction problems occurring in entry flights into Earth, Mars, Venus, Titan, and outer planets.

1.0 NOMENCLATURE

B	: Rotational constant, cm^{-1} .
c	: Speed of sound, m/s .
(c)	: Crystalline (solid) state.
C	: Average molecular speed ($\sqrt{8kT/\pi m}$), m/s .
C_p	: Specific heat at constant pressure, $\text{J}/(\text{kg}\cdot\text{K})$.
C_v	: Specific heat at constant volume, $\text{J}/(\text{kg}\cdot\text{K})$.
D	: Effective diffusion coefficient.
D_a	: Adsorption energy, J/mol .
D_b	: Diffusion barrier energy, J/mol .
D_g	: Dissociation energy in gas phase, J/mol .
$D_{i,s}$: Multicomponent diffusion coefficient between species i and s , m^2/sec .
f	: Stream function, Eq. (32).
F_s	: A bifurcation parameter, Eq. (44), dimensionless.
g	: Normalized energy, Eq. (36).
H	: Enthalpy, J/kg .
ΔH	: Energy produced by reaction, eV or J/mol .
J_s	: Rate of mass diffusion of species s , $\text{kg}/(\text{m}^2\cdot\text{sec})$.
k	: Boltzmann constant, J/K .
k_w	: Catalytic velocity, Eq. (5), m/s .
m	: Mass of one unspecified particle, kg .
m_s	: Mass of one particle of species s , kg .
\dot{m}_p	: Pyrolysis gas mass flow rate, $\text{kg}/(\text{m}^2\cdot\text{sec})$.
$\dot{m}_{p,s}$: Mass flow rate of species s in pyrolysis gas, $\text{kg}/(\text{m}^2\cdot\text{sec})$.
$\dot{m}_{t,s}$: Mass flow rate of species s resulting from reactions and sublimation, $\text{kg}/(\text{m}^2\cdot\text{sec})$.
\dot{m}_t	: Mass flow rate of material removed by surface reaction and sublimation, $\text{kg}/(\text{m}^2\cdot\text{sec})$.
$\dot{m}_{v,s}$: Mass flow rate of species s in sublimation product, $\text{kg}/(\text{m}^2\cdot\text{sec})$.
M_s	: Molecular weight of species s , kg/mol .
\bar{M}	: Average molecular weight, kg/mol .
M_w	: V_∞/c_w , dimensionless.
n_a	: Number density of adsorbed molecules, m^{-2} .
n_g	: Number density of gas molecules, m^{-3} .
N	: Number of species.
p	: Pressure, Pascal.
Pr	: Prandtl number, dimensionless.
q	: Heat transfer rate, W/m^2 .

Park, C. (2007) Numerical Implementation of Surface Catalysis, Reaction, and Sublimation. In *Experiment, Modeling and Simulation of Gas-Surface Interactions for Reactive Flows in Hypersonic Flights* (pp. 16-1 – 16-20). Educational Notes RTO-EN-AVT-142, Paper 16. Neuilly-sur-Seine, France: RTO. Available from: <http://www.rto.nato.int/abstracts.asp>.

Q	: Partition function.
r	: Radial distance from axis of symmetry, m.
R	: Nose radius, m.
Re_∞	: Freestream Reynolds number $\rho_\infty V_\infty R / \mu_\infty$.
$S(c)$: Unspecified solid surface.
Sc	: Schmidt number, dimensionless.
T	: Temperature, K.
u	: Tangential velocity, m/s.
v	: Normal velocity, m/s.
V_∞	: Freestream velocity, m/s.
x	: Distance along wall measured from the stagnation point, m.
W_s	: Rate of production of species s , sec^{-1} .
X_s	: Molar fraction of species s .
y	: Distance normal to wall measured from wall, m.
Z_s	: Virtual species mass fraction in bifurcation model, Eq. (47).
α_s	: Mass fraction of species s , dimensionless.
γ	: C_p/C_v .
ϕ	: Roughness ratio (BET area/projected area), dimensionless.
η	: Boundary layer coordinate normal to wall, Eq. (31b), dimensionless.
η_a	: Adsorption (sticking) coefficient, dimensionless.
η_c	: Catalytic recombination coefficient, dimensionless.
η_r	: Reaction coefficient, dimensionless.
η_v	: Evaporation coefficient, dimensionless.
μ	: Viscosity, m^2/sec .
μ_1	: A bifurcation parameter, Eq. (48a), dimensionless.
μ_2	: A bifurcation parameter, Eq. (48b), dimensionless.
ρ	: Density, kg/m^3 .
ξ	: Boundary layer coordinate along wall, Eq. (31a), dimensionless.

1.1. SUPERScript

' : $\partial/\partial\eta$.

1.2. SUBSCRIPTS

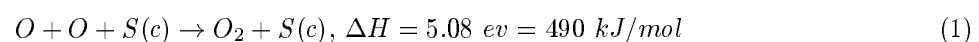
∞	: Freestream.
a	: Adsorbed state.
e	: Edge of boundary layer.
E	: Equilibrium.
$,f$: Forward reaction.
g	: Gas.
$,r$: Reverse reaction.
R	: Rotational mode.
T	: Translational mode.
v	: Evaporation.
V	: Vibrational mode.
w	: Wall.

2.0 PHYSICS OF GAS-SURFACE INTERACTIONS

2.1. GOULARD'S WORK ON CATALYTIC EFFECTS

The problem of chemical reactions at a solid surface was made aware first by Goulard.¹ He pointed out that, in an environment where chemical reactions are frozen in the boundary layer, heat transfer rate q to the wall can be reduced by making it noncatalytic to recombination. In most practical flight regimes of hypersonic vehicles, boundary layer flows are indeed chemically frozen. The flight experiments conducted with the Space Shuttle proved Goulard's thesis.

Goulard considered the catalytic recombination process typified by ($1 \text{ ev} = 96.48 \text{ J/mol}$)



in the stagnation region shown schematically in Fig. 1. Here, S(c) signifies that the phenomenon occurs at the surface of an unspecified material (c here signifies crystalline state). His work introduced three important axioms. The first axiom is that the ratio of heat transfer rates between a fully catalytic and noncatalytic surfaces is approximately the ratio of the total, i.e., translational (CpT) plus chemical, enthalpy to the translation-only enthalpies.

$$\frac{q \text{ to fully catalytic wall}}{q \text{ to noncatalytic wall}} \approx \frac{CpT + \text{energy contained in dissociation}}{CpT} \quad (2)$$

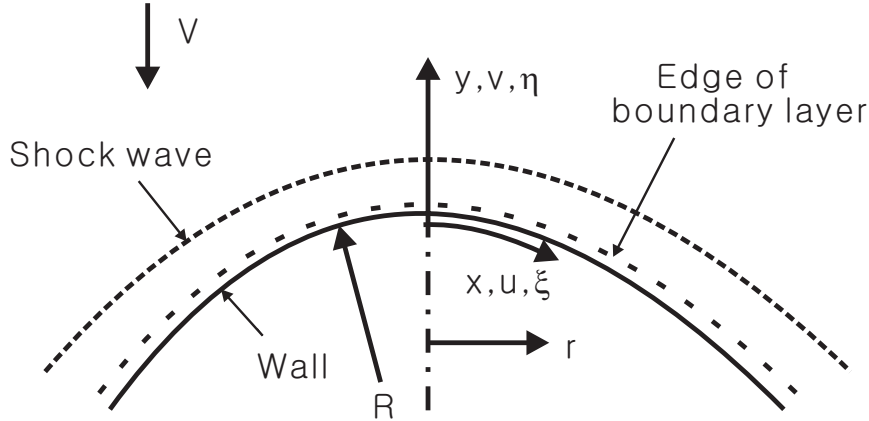


Figure 1. Flowfield considered by Goulard.¹

The second axiom is that the heat transfer rate to the fully catalytic wall is approximately the same as that in a nonreacting gas:

$$q \text{ to a fully catalytic wall} \approx q \text{ in a nonreacting gas.} \quad (3)$$

The third axiom is that the transition from the noncatalytic to catalytic surface occurs at around the point where the quantity

$$\zeta = \frac{0.47}{Sc^{2/3}} \frac{1}{\rho_w k_w} \sqrt{2\rho_e \mu_e \left(\frac{du_e}{dx}\right)} \quad (4)$$

becomes unity. Here k_w is the so-called catalytic velocity defined as

$$k_w = \frac{\eta_{c,f}}{4} C_w = \frac{\eta_{c,f}}{4} \sqrt{\frac{8kT_w}{\pi m}} = \frac{\eta_{c,f}}{4} \sqrt{\frac{8}{\pi\gamma}} c_w \approx 0.34\eta_{c,f}c_w \quad (5)$$

where $\eta_{c,f}$ is the recombination coefficient, i.e., the fraction of the colliding reactive species (e.g., atomic oxygen) that undergoes the recombination process. The subscript “,f” signifies that the coefficient is for the forward process, to distinguish it from the reverse process. The quantity γ is the specific heat ratio, Cp/Cv , and c is the sound speed. γ is taken to be 1.4 to arrive at the factor 0.34 in Eq. (5). The quantity k_w has its origin in the kinetic theory. In kinetic theory, the number of atoms or molecules hitting a surface is given by the so-called arrival rate

$$\text{Arrival rate} = \frac{n}{4} C = \frac{n}{4} \sqrt{\frac{8kT}{\pi m}} \quad m^{-2}sec^{-1} \quad (6)$$

where n is the number density in m^{-3} . The subscripts e and w in Eq. (4) signify the edge of boundary layer and wall, respectively.

The dependence of heat transfer rate on ζ is

$$\frac{q - q_{noncatalytic}}{q_{fullycatalytic} - q_{noncatalytic}} = \frac{1}{1 + \zeta}.$$

This produces a curve known as Goulard’s S-curve, which is shown in Fig. 2.

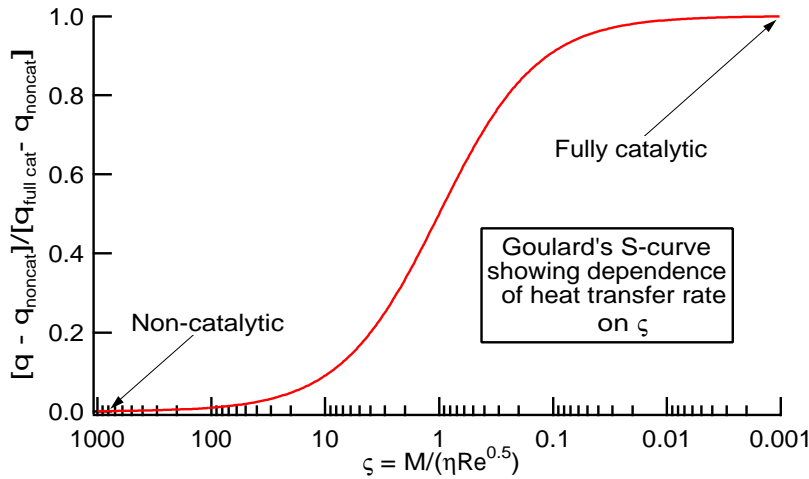


Figure 2. Goulard's S-curve dependence of heat transfer rate on ζ .

By assuming that the pressure distribution in the stagnation region is that given by the Newtonian hypersonic theory, the quantity du_e/dx is found approximately to be

$$\frac{du_e}{dx} = \frac{V_\infty}{R} \sqrt{2 \frac{\rho_\infty}{\rho_e}}. \quad (7)$$

A typical value of ζ can be found by taking $Sc = 0.5$, $T_\infty = 250$ K, $T_e = 6000$ K, $T_w = 3000$ K, $\rho_\infty/\rho_e = 1/10$, $\mu \propto T^{3/4}$, $\gamma = 1.4$, and defining the freestream Reynolds number

$$Re_\infty = \frac{\rho_\infty V_\infty R}{\mu_\infty},$$

which leads to, to within about 30% accuracy,

$$\zeta \approx \frac{1}{\eta_{c,f}} \frac{V_\infty}{c_w} \frac{1}{\sqrt{Re_\infty}}. \quad (8)$$

Writing the ratio V_∞/c_w as M_w , the freestream Mach number evaluated at the wall temperature, a fully catalytic surface and a noncatalytic wall can be defined as

$$\text{Fully catalytic wall : } \eta_{c,f} \sqrt{Re_\infty} \gg M_w \quad (8a)$$

$$\text{Noncatalytic wall : } \eta_{c,f} \sqrt{Re_\infty} \ll M_w. \quad (8b)$$

Using arc-heated wind tunnels, $\eta_{c,f}$ for the $O + O \rightarrow O_2$ and $N + N \rightarrow N_2$ reactions have been measured for several common heatshield materials. Generally, it is between 0.1 and 1 for a metal, between 0.01 and 0.1 for a metal oxide, and less than 0.01 for silica and alumina, two most commonly found glassy oxides.

It is to be noted here that the surface of most innoble metals, such as copper, turns quickly into a metal oxide when it is exposed to a hot stream containing atomic oxygen. A systematic study was made in Ref. 2 to find out how fast a copper surface turns into a copper oxide surface. The experiment was made at a pressure of the order of 0.01 atm. Within 1 sec at this pressure, copper became copper oxide when it was tested in an arc-heated wind tunnel. In Ref. 3, copper calorimeter was used to measure the heat transfer rate at a pressure of 2/3 atmospheres. In this case, enthalpy of the flow was determined spectroscopically. The measured heat transfer rate to the copper calorimeter was consistent with the assumption that $\eta_{c,f}$ is 0.01, which is a typical value for metal oxides.

Of particular interest is the $\eta_{c,f}$ value for O-atoms on the surface of graphitic carbon, which is used as an ablative heatshield. Efforts have been made in the past to measure this quantity in an

atomic beam experiment (see, e.g., Ref. 4). Those experiments found no O₂ in the product: the O-atoms either formed CO by combining with carbon or reflected elastically as an O-atom, without forming O₂. That is,

$$\text{For } O + O + C(c) \rightarrow O_2 + C(c) : \eta_{c,f} \approx 0. \quad (9)$$

2.2. $\eta_{c,f}$ FOR $CO + O \rightarrow CO_2$

When unmanned Mars entry missions were started, question was raised as to what is the impact of surface catalytic recombination. Martian atmosphere consists mostly of CO₂. At the edge of boundary layer, CO₂ is fully dissociated into CO and O. CO and O could conceivably recombine as



At a flight velocity of 6 km/s, a typical entry velocity of a Martian vehicle, the kinetic energy of one CO₂ molecule is 8.21 ev. Therefore the reaction energy 5.35 ev is more than half of the flow enthalpy. If CO and O do not recombine catalytically at wall, Eq. (1) tells us that the heat transfer rate will be less than half of the fully catalytic case. That is, reward to making the wall noncatalytic is quite large. The same problem exists for Venusian entry because the atmospheric composition of Venus is similar to that of Mars.

Automobile manufacturers have developed catalytic converters which burn CO with O₂ to make CO₂. They accomplished it by making CO molecules collide many times with platinum surfaces in the presence of O₂. This means that the catalytic efficiency $\eta_{c,f}$ is very small for CO + O₂. NASA Ames Research Center carried out an experiment to measure $\eta_{c,f}$ for the CO + O reaction. Because the surface of the heatshield for Martian entry vehicle is usually fused silica, the experiment was conducted for the silica surface.⁵ The experiment found that the reaction CO + O is too slow to be detected.

That $\eta_{c,f}$ for CO + O → CO₂ is small can be deduced theoretically. A catalytic reaction involves: 1) adsorption (sticking) of the two component species, 2) migration of the component species in the adsorbed phase, 3) recombination of the two partners, and 4) desorption of the product. The CO and O particles that strike the wall may not be adsorbed, i.e., fail step 1), or, skip step 3) and desorb without recombining. The rates of these four processes can be modeled. That work will be done by author lecturers. Here, only the steps 1) and 4) will be given to explain why $\eta_{c,f}$ for the process is slow.

The $\eta_{c,f}$ for the catalytic process cannot be larger than the adsorption coefficient of CO, because the latter is a component of the former. For a monatomic gas, the adsorption coefficient, denoted here η_a , is known to be a function of the ratio of the mass of the gas atom m_g to that of the atoms forming the solid m_c . Classical calculation of the surface processes⁶ predict that, when the mass ratio is much smaller than unity, η_a behaves as

$$\eta_a \approx \sqrt{m_g/m_c}.$$

The existing experimental data with helium, neon, and argon⁷ agree roughly with this theory.

As mentioned, the surface of the heatshield for the Martian entry vehicles is usually SiO₂. Because the molecular weight of Si is 28, collisions of the CO and O will have little effect of this mass ratio. Thus, in the absence of other effects, η_a should be nearly 1 in the Martian case.

But there is what is known as entropy effect, which concerns the change in the internal degrees of freedom during adsorption. (To change internal degrees of freedom, heat must be given or taken away at a constant temperature. By the definition of entropy, this implies a change in entropy.) Let us designate the gas phase quantities by a subscript g and the adsorbed state quantities by a subscript a . The adsorbed gas species are held there by the attractive potential between the solid surface and the gas, D_a . The numerical value of D_a is known for some cases⁸. For CO on a metal, it is typically between 1.5 and 6 ev.

A molecule in the adsorbed state oscillates within the adsorption potential well approximately with the same frequency as the solid lattice, which is $\nu \approx kT_w/h$ on the average. The fraction of the adsorbed CO molecules that has an energy exceeding the adsorption energy D_a is $\exp(-D_a/kT_w)$.

Therefore, the number of CO molecules in the adsorbed state that desorb from the adsorption potential well within 1 sec per 1 m² is

$$\text{Desorption rate} = \frac{kT_w}{h} \exp\left(-\frac{D_a}{kT_w}\right) n_a \quad \text{m}^{-2} \text{sec}^{-1}$$

As given by Eq. (6), the flux of gas-phase molecules reaching the wall is $C_w n_g / 4$. Only the η_a fraction of this flux will be adsorbed, so that

$$\text{Adsorption rate} = \frac{\eta_a}{4} C_w n_g \quad \text{m}^{-2} \text{sec}^{-1}.$$

Under equilibrium, these two rates must be equal, i.e.,

$$\frac{kT_w}{h} \exp\left(-\frac{D_a}{kT_w}\right) n_{aE} = \frac{\eta_a C_w}{4} n_g$$

which leads to

$$\eta_a = \frac{4}{C_w} \frac{kT_w}{h} \exp\left(\frac{D_a}{kT_w}\right) \frac{n_{aE}}{n_g}.$$

The ratio n_{aE}/n_g is given by the partition functions for translation Q_T , for vibration Q_v , and for rotation Q_r , by

$$\frac{n_{aE}}{n_g} = \frac{Q_{Ta} Q_{Va} Q_{Ra}}{Q_{Tg} Q_{Vg} Q_{Rg}} \exp\left(\frac{D_a}{kT_w}\right).$$

Therefore

$$\eta_a = \frac{4}{C_w} \frac{kT_w}{h} \frac{Q_{Ta} Q_{Va} Q_{Ra}}{Q_{Tg} Q_{Vg} Q_{Rg}}.$$

Here, all partition functions are evaluated at the wall temperature T_w .

The translational partition function in the gas phase, Q_{Tg} , is given by

$$Q_{Tg} = \left(\frac{2\pi mkT_w}{h^2}\right)^{3/2}$$

The largest possible value of the translational partition function in the adsorbed phase, Q_{Ta} , occurs when the adsorbed molecule has a full freedom of translation in two dimensions, in which case

$$Q_{Ta}(\text{full } 2D) = \frac{2\pi mkT_w}{h^2}.$$

When there is an energy barrier of D_b that hinders the two-dimensional motion, so that only those molecules with energy greater than D_b have the two-dimensional translational freedom, one must multiply a factor $\exp(-D_b/kT)$ to this value, and therefore

$$Q_{Ta} = \frac{2\pi mkT_w}{h^2} \exp\left(-\frac{D_b}{kT_w}\right). \quad (10)$$

This leads to

$$\eta_a = \frac{4}{C_w} \frac{kT_w}{h} \left(\frac{h^2}{2\pi mkT_w}\right)^{1/2} \frac{Q_{Va} Q_{Ra}}{Q_{Vg} Q_{Rg}} \exp\left(-\frac{D_b}{kT_w}\right) = \frac{Q_{Va} Q_{Ra}}{Q_{Vg} Q_{Rg}} \exp\left(-\frac{D_b}{kT_w}\right). \quad (11)$$

For a monatomic gas, Q_v and Q_r are both unity. If $D_b = 0$, Eq. (11) gives $\eta_a = 1$. This agrees with what is known about η_a for monatomic species.

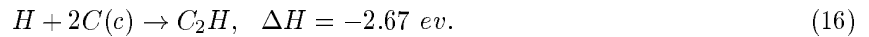
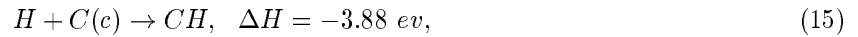
At best, the rotational motion of an adsorbed molecule occurs around only one axis, the axis normal to the surface. By assuming that the vibrational motion of the adsorbed phase is excited to the same extent as the gas phase, one obtains the largest possible value of the adsorption coefficient to be

$$\eta_a = \sqrt{\frac{B}{kT_w}} \exp\left(-\frac{D_b}{kT_w}\right) \quad (12)$$

Assuming $D_a = 0$, the numerical value of η_a for CO at the wall temperature of 2000 K is deduced to be 0.0373. If D_a is finite, or the rotational motion is hindered completely, or if the vibrational motion is hindered in the adsorbed phase, η_a will be smaller. This explains at least partly why the catalytic recombination coefficient for $\text{CO} + \text{O}$ is small on the surface of SiO_2 .

2.3. GAS-SOLID REACTIONS AND SUBLIMATION

At high heating rates, the heatshield surfaces ablate. For an ablating environment, carbonaceous heatshield is commonly used. For this case, the gas species O, N, and H can combine with the carbon atoms of the solid surface as



For reaction (13), the existing experimental data⁹ show that the reaction coefficient $\eta_{r,f}$ can be approximated by

$$\text{O} + \text{C}(c) \rightarrow \text{CO} : \eta_{r,f} \approx 0.63 \exp(-1160/T_w).$$

For reaction (14), Ref. 10 shows

$$\text{N} + \text{C}(c) \rightarrow \text{CN} : \eta_{r,f} \approx 0.3.$$

Reactions (15) and (16) can occur only at high wall temperatures, and have not yet been studied. However, the maximum possible values can be reasoned simply from the requirement that only the particles with the required energies (3.88 ev for $\text{H} + \text{C}(c)$ and 2.67 ev for $\text{H} + 2\text{C}(c)$) can produce the change. This leads to

$$\text{H} + \text{C}(c) \rightarrow \text{CH} : \eta_{r,f} < \exp(-45,000/T_w)$$

$$\text{H} + 2\text{C}(c) \rightarrow \text{C}_2\text{H} : \eta_{r,f} < \exp(-31,000/T_w).$$

If the flow contains CH or C_2H at the boundary layer edge, as in the atmosphere of Titan, reactions (15) and (16) will occur in the reverse direction at wall. That is, carbon will condense on the wall from CH and C_2H .

At high wall temperatures, evaporation (sublimation if the surface is solid) occurs. Imagine that a wall material is enclosed in a high temperature furnace and is heated. Evaporation will occur and fill the inside volume with the vapor of the material. The equilibrium vapor pressure for most materials are known, and are given in the JANAF Thermochemical Tables.¹¹ Denoting the equilibrium vapor number density by n_E , the flux of the vapor species hitting the wall is given by the kinetic theory to be $n_E C_w/4$. Of this flux, in general an η_v fraction will be adsorbed on the wall. Under equilibrium, this flux must equal the flux of evaporation. Thus the evaporation rate is given by $\eta_v n_E C_w/4$. Under nonequilibrium, the vapor number density n will produce adsorption rate of $\eta_v n C_w/4$. Therefore, the net mass flux of evaporation will be

$$\text{Evaporating flux} = \frac{\eta_v}{4} C_w (n_E - n) \text{ m}^{-2} \text{ sec}^{-1}$$

where n_E and n are evaluated at the wall. The corresponding mass flux becomes, in terms of mass fraction α ,

$$J = \frac{\eta_v}{4} \rho_w C_w (\alpha_E - \alpha) \text{ kg}/(\text{m}^2 - \text{sec}) \quad (17)$$

Graphitic carbon vaporizes into C, C_2 , C_3 , C_4 , and C_5 . Of these, the predominant reaction is



For this process, η_v has been measured in Ref. 12. The results can be fitted by

$$\eta_v(C_3) = 30 \exp(-21490/T_w).$$

Glassy oxides liquefy before they vaporize. Vaporization of liquid oxides involves at least two steps. For instance, when SiO_2 is heated, its vapor consists of SiO and O_2 . No quantitative information is available for η_v for this class of materials.

2.4. ROUGH SURFACES

When the surface reaction of the type Eqs. (13) to (16) or vaporization, Eq. (18), occurs, the surface becomes rough. The extent of roughness is measured by the ratio of the so-called BET (Bennett-Emmons-Thomas) area to the projected area, named here ϕ

$$\text{Roughness ratio } \phi = \frac{\text{BET area}}{\text{projected area}}. \tag{19}$$

BET area is the wet area of a substance, and is determined by an experiment shown schematically in Fig. 3. One places the sample inside a sealed jar and evacuates the jar. The sample is heated while pumping to purge all gas molecules adsorbed on it. Then one admits gas, typically nitrogen, while measuring the mass flow rate that enters the jar and watching the pressure inside the jar. In the beginning, pressure in the jar does not rise because all gas molecules are consumed in adsorbing on the wet surface of the sample. After a while, pressure begins to rise, because the surface is fully covered by a monolayer of the adsorbed gas. The surface area occupied by one molecule is typically 10^{-15} cm^2 . By dividing the total number of gas molecules consumed up to this point by this value, one obtains the BET area.

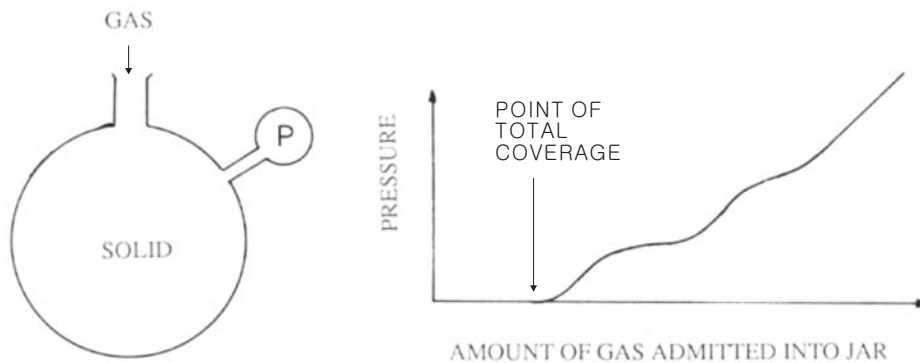


Figure 3. Schematic of the procedure to determine the BET area of a solid surface.

The BET area has never been measured during ablation. After ablation, theoretically it can be measured. However, a heatshield material becomes highly porous after ablation. The experiment shown in Fig. 3 will measure the wet area of the pores as well as the area exposed to the boundary layer flow. Therefore, the roughness ratio ϕ can only be guessed. For many such porous materials, ϕ is of the order of 100. Perhaps we should consider ϕ to be between 10 and 100.

We can now conduct a thought experiment as to what will be the magnitude of the adsorption coefficient η_a on a rough surface, as shown schematically in Fig. 4. Here, a swarm of atoms is hitting the inside of a crevice. In the first collision, η_a fraction is adsorbed, and $1 - \eta_a$ fraction leaves. This remaining swarm of atoms hits the wall the second time. The atoms that leave are now $(1 - \eta_a)^2$ fraction of the original swarm. After n number of collisions, there will be $(1 - \eta_a)^n$ fraction of the original swarm left unadsorbed. Therefore, the fraction of the atoms adsorbed are

$$\text{Effective adsorption coef} = 1 - (1 - \eta_a)^n. \tag{20}$$

The total number of collisions, n , will be of the order of ϕ . So, to this order of accuracy, n can be replaced by ϕ . If η_a is very small and if ϕ is large, Eq. (20) can be approximated by

$$\text{Effective adsorption coef} \approx 1 - \exp(-\eta_a \phi). \tag{21}$$

These show that, when a surface is rough, its effective η_a approaches unity.

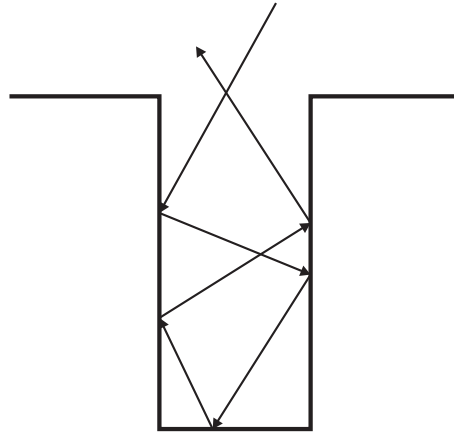


Figure 4. Schematic showing collisions of particles on a rough surface.

2.5. INTER-RELATIONSHIP AMONG η 's

The above reasoning can be applied to catalytic reactions and surface reactions to conclude that not only η_a , but η_c , η_r , and η_v all approach unity when roughness ratio is high. However, all η 's cannot become unity together because, by definition, the sum of all η 's for one species must not be larger than unity:

$$\Sigma \eta < 1. \quad (22)$$

Otherwise, mass conservation is violated.

Take an example with O-atoms hitting a carbon surface. O-atoms can possibly recombine on the surface with a coefficient $\eta_{c,f}$ and simultaneously can react with carbon to form CO with a coefficient $\eta_{r,f}$. The sum, $\eta_{c,f} + \eta_{r,f}$, cannot be larger than unity. Because $\eta_{c,f}$ is nearly zero and $\eta_{r,f}$ is large, the best practice may be to take the effective $\eta_{r,f}$ to be unity and the effective $\eta_{c,f}$ to be 0 for a rough carbon surface.

2.6. FORWARD VS. REVERSE RATES

In Eq. (17), the two terms in the parenthesis represent the forward and reverse rates in evaporation. Likewise, for both the catalytic recombination processes typified by Eq. (1) and the surface reactions, Eqs. (13) to (16), the reverse rates must be accounted for. The reverse rates are chosen so as to satisfy the principle of detailed balance in equilibrium. Otherwise, equilibrium condition will not be reached when it should be. This aspect of the problem is discussed in Ref. 13.

For example, let us take the recombination process, Eq. (1). There is an opposing (reverse) reaction



The fraction of the O_2 molecules that undergoes this process will be designated by $\eta_{c,r}$. The net reaction rate will be the difference between the forward and the reverse rates

$$\text{Net rate of O removal} = \frac{\eta_{c,f}}{4} C_{w,O} n_O - 2 \frac{\eta_{c,r}}{4} C_{w,O_2} n_{O_2} \quad m^{-2} sec^{-1}.$$

Here, the factor 2 in the second term signifies that two O-atoms are created by the dissociation of one O_2 molecule. The mass flux of the O-atoms removed by this process can be written as

$$J_O = \frac{1}{4} \rho_w (\eta_{c,f} C_{w,O} \alpha_{O,w} - 2 \eta_{c,r} C_{w,O_2} \alpha_{O_2,w}). \quad (24)$$

Under equilibrium, the forward and reverse rates must be equal, which leads to

$$\eta_{c,r} = \frac{\eta_{c,f}}{2} \frac{C_{w,O}}{C_{w,O_2}} \frac{n_{O,E}}{n_{O_2,E}} = \frac{1}{\sqrt{2}} \eta_{c,f} \left(\frac{n_O}{n_{O_2}} \right)_E. \quad (25)$$

The ratio $n_{O,E}/n_{O_2,E}$ is given by the equilibrium relationship

$$\left(\frac{n_O}{n_{O_2}}\right)_E = \frac{(Q_{T,O})^2}{Q_{T,O_2}Q_{V,O_2}Q_{R,O_2}} \exp\left(-\frac{D_g}{kT_w}\right),$$

from which there results

$$\left(\frac{n_O}{n_{O_2}}\right)_E = \frac{1}{n_O} \frac{(Q_{T,O})^2}{Q_{T,O_2}Q_{V,O_2}Q_{R,O_2}} \exp\left(-\frac{D_g}{kT_w}\right). \quad (26)$$

A similar relation holds for all other catalytic recombination processes.

Similarly, for the surface reaction (13), the net rate is

$$\text{Net rate of O removal} = \frac{\eta_{r,f}}{4} C_{w,O} n_O - \frac{\eta_{r,r}}{4} C_{w,CO} n_{CO} \quad m^{-2} sec^{-1}$$

or

$$J_O = \frac{1}{4} \rho_w (\eta_{r,f} C_{w,O} \alpha_{O,w} - \eta_{r,r} C_{w,CO} \alpha_{CO,w}) \quad kg/(m^2 - sec). \quad (27)$$

Here

$$\eta_{r,r} = \eta_{r,f} \frac{C_{w,O}}{C_{w,CO}} \left(\frac{n_O}{n_{CO}}\right)_E. \quad (28)$$

The ratio $(n_O/n_{CO})_E$ is given by the equilibrium relationship

$$\left(\frac{n_O}{n_{CO}}\right)_E = \frac{1}{n_{C,E}} \frac{Q_{T,O}Q_{T,C}}{Q_{T,CO}Q_{V,CO}Q_{R,CO}} \exp\left(-\frac{D_g}{kT_w}\right). \quad (29)$$

where $n_{C,E}$ is the equilibrium vapor number density of C_3 . A similar relationship holds for all other surface reactions.

2.7. HEAT TRANSFER RATES

All three surface phenomena, i.e. catalytic recombination, reaction, and sublimation, produce heat corresponding to ΔH . All these heat enter into the heatshield wall. The heat transfer rate caused by these phenomena are

$$q = \text{Rate of reaction in } \frac{\text{event}}{m^2 sec} \times \frac{\Delta H \text{ in J/mol}}{6.0225 \times 10^{23}} \quad W/m^2. \quad (30)$$

Here, one must not confuse event/(m²sec) with rate of species removal or species production. For instance, for the oxygen recombination, Eq. (9), removal of two atomic oxygen equals one event. Therefore, event/(m²sec) is half of the rate of removal of O-atoms. The above equation is valid unconditionally, regardless of the magnitude of ablation rate.

2.8. EXTENSION OF GOULARD'S THIRD AXIOM

We can now ponder how much impact the coefficients η_r (in the surface reactions of the form (13) to (16)) and η_v (in sublimation of the form (18)) will have on heat transfer at the stagnation point. In other words, we would like to extend Goulard's analysis to surface reactions and sublimation. Unlike catalytic recombination process, surface reaction and sublimation produce ablation. To extend Goulard's theory to an ablating surface, we have to start with the fundamental conservation equations.

Fundamental conservation equations for the frozen boundary layer flow are given in Goulard's work¹, and so will not be repeated here. Those equations are valid even when surface reactions and sublimation occur. Following Goulard, we write those conservation equations using the coordinates x and y shown in Fig. 1. Then one introduces the coordinate transformation

$$\xi = \int_0^x \rho_e \mu_e u_e r^2 dx, \quad \eta = \frac{r u_e}{\sqrt{2\xi}} \int_0^y \rho dy, \quad (31a, b)$$

and the stream function f that satisfies the conditions

$$\frac{\partial \Psi}{\partial y} = \rho u r, \quad \frac{\partial \Psi}{\partial x} = -\rho v r$$

$$\Psi = \sqrt{2\xi} f(\xi, \eta). \quad (32)$$

The stream function f can be written as

$$f = -\frac{\rho v}{\sqrt{2\rho_e \mu_e} (du_e/dx)}. \quad (33)$$

Then, denoting the partial differentiation $\partial/\partial\eta$ by $'$, the mass and momentum conservation equations reduce to:

$$\left(\frac{\rho\mu}{\rho_e\mu_e} f''\right)' + f f'' + \frac{1}{2}\left(\frac{\rho_e}{\rho} - f'^2\right) = 0. \quad (34)$$

Following Goulard, we assume $\rho_e/\rho = f'^2$, so that Eq. (34) reduces further to

$$\left(\frac{\rho\mu}{\rho_e\mu_e} f''\right)' + f f'' = 0. \quad (35)$$

The energy equation is transformed likewise by introducing a normalized energy function

$$g = H/H_e \quad (36)$$

into

$$\left(\frac{\rho\mu}{\rho_e\mu_e} \frac{1}{Pr} g'\right)' + f g' + \frac{u_e^2}{H_e} \left[\left(1 - \frac{1}{Pr}\right) \frac{\rho\mu}{\rho_e\mu_e} f' f''\right]' = 0. \quad (37)$$

Assuming Prandtl number to be unity, Eq. (37) reduces further to

$$\left(\frac{\rho\mu}{\rho_e\mu_e} \frac{1}{Pr} g'\right)' + f g' = 0. \quad (38)$$

The species equation is transformed likewise into

$$\left(\frac{\rho\mu}{\rho_e\mu_e} \frac{1}{Sc} \alpha'_s\right)' + f \alpha'_s = 0 \quad (39)$$

When there is no ablation, the wall value of f is zero according to Eq. (33). The numerical value of 0.47 appearing in Goulard's parameter ζ , Eq. (4), is the wall slope of species mass fraction α in the solution of Eq (39), $(\partial\alpha/\partial\eta)_w$, for $Sc = 1$. 0.47 also happens to be the wall slope of the energy variable in Eq. (38), $(\partial g/\partial\eta)_w$, for $Pr = 1$.

When there is ablation, the wall value of f

$$f_w = -\frac{\rho_w v_w}{\sqrt{2\rho_e \mu_e} (du_e/dx)}. \quad (40)$$

is no longer zero, but is finite negative. When f_w has a finite negative value, numerical value of $(\partial\alpha/\partial\eta)_w$ and $(\partial g/\partial\eta)_w$ are different from 0.47. Numerical solution of those differential equations give these wall slope values as shown in Fig. 5. A two-parameter fit

$$\left(\frac{\partial g}{\partial\eta}\right)_w = \left(\frac{\partial\alpha}{\partial\eta}\right)_w = 0.47 \exp(0.467 f_w - 4.017 f_w^2) \quad (41)$$

is shown in the figure for comparison. The analytical fit is seen to be valid to f_w of up to about -1.2.

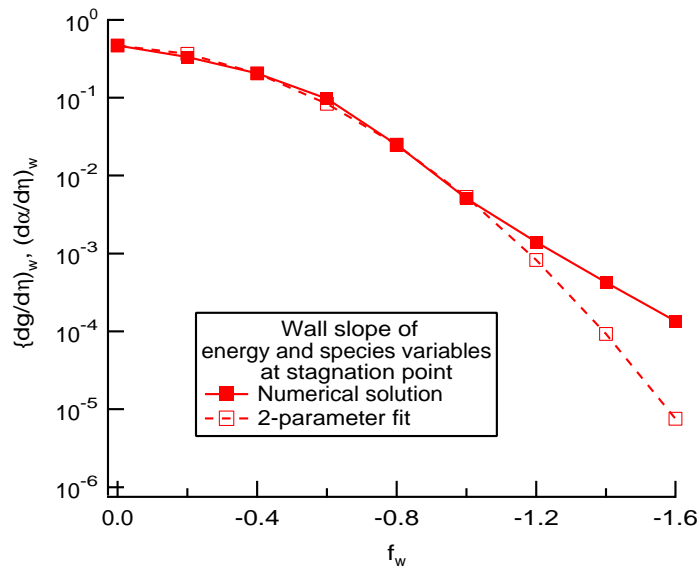


Figure 5. Wall slope of energy and species equations at the stagnation point, under Goulard’s simplifications.

The wall slope of the energy equation, $(\partial g/\partial \eta)_w$, is a measure of heat transfer rate. As Fig. 5 shows, it decreases rapidly as $-f_w$ increases. This phenomenon is known as convective blockage effect. Using Eq.(7), f_w can be written as

$$f_w = -\frac{\dot{m}}{\rho_\infty V_\infty} 2^{-3/4} \left(\frac{\rho_\infty}{\rho_e}\right)^{1/4} \sqrt{Re_\infty},$$

where \dot{m} is the rate of mass injection by ablation. Taking ρ_∞/ρ_e to be 0.1, this becomes

$$f_w \approx -0.33 \frac{\dot{m}}{\rho_\infty V_\infty} \sqrt{Re_\infty}. \tag{42}$$

The quantity f_w is the fundamental quantity in the so-called blowing parameter, which is a ratio of the mass injection rate \dot{m} and the freestream flow rate $\rho_\infty V_\infty$ and which is defined slightly differently by various researchers.

By replacing 0.47 in Goulard’s ζ , Eq. (4), by the expression (41), one has Goulard’s third axiom extended to the case of finite ablation rate. Generally, finite f_w pushes the S-curve in Fig. 2 toward the right, so that the wall behaves more as a catalytic wall for the same catalytic coefficient.

The S-curve can be used also to gage the impacts of surface reactions or sublimation on heat transfer. For instance, if there was surface reaction of the form Eq. (13) but no surface catalysis or sublimation, heat transfer rate will increase due to the surface reaction. The S-curve in Fig. 2 is applicable exactly as it is. However, the magnitude of the heat transfer rate will have to be changed using the curve shown in Fig. 5.

3.0. KINETIC BOUNDARY CONDITIONS

3.1. BIFURCATION MODEL

When the heating rate is above about 500 kW/m², a heatshield material loses mass during heating. That is, it is not truly reusable. Between about 500 kW/m² and 1.5 MW/m², the mass loss rate is so small that the material can be replenished after use, to be used the next time. When the heating rate exceeds about 1.5 MW/m², the mass loss rate is so high that an ablating material must be used. An ablating material consists generally of two components, a highly temperature-resistant, highly tensile-resistant fibre matrix and a resin. The material is usually porous. When it is heated, resin vaporizes at relatively low temperatures, e.g., 500 K. The vapor passes through the pores and escapes from the surface (see Fig. 6). The vaporization process absorbs heat. While passing through

the pores, the vapor molecule decomposes into smaller molecules. This decomposition process absorbs heat and thereby cools the material further. This gas is called pyrolysis gas, and the process is called pyrolysis process. In the region near the wall surface, the matrix is devoid of the resin. This region is called char. The zone where the vaporization of the resin is occurring is called the pyrolysis zone.

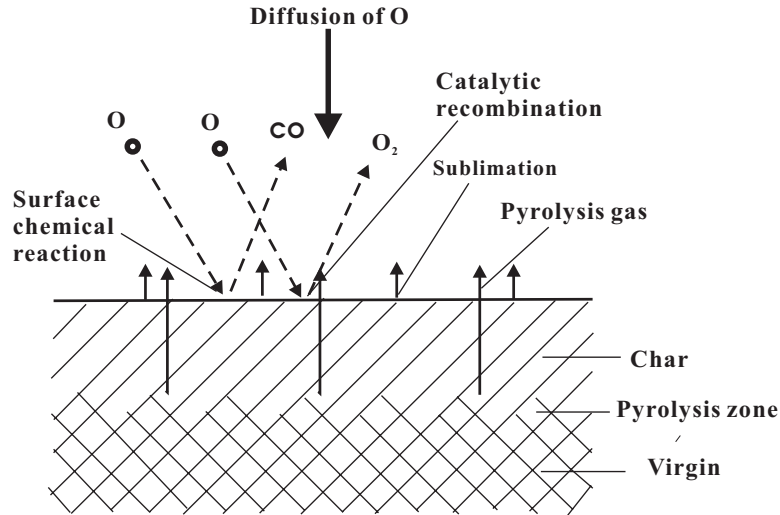


Figure 6. Schematic of the phenomena occurring below, at, and above the wall surface of an ablating heatshield.

The general principle of mass balance at wall states that whatever is produced or removed at wall is taken away or supplied by diffusion in the boundary layer, i.e.

$$\text{Rate of production at wall} = \text{rate of removal by diffusion.} \quad (43)$$

Therefore, before proceeding any further, we must know how to express the rate of diffusion.

The rate of diffusion of a species is given in general by the Chapman-Enskog theory using the multi-component diffusion coefficients. According to this formulation, the rate of diffusion of species s is a weighted sum of gradients, $\partial X_i / \partial y$, of all species except s . The weights contain the multi-component diffusion coefficients D_{is} as a factor. This complicates wall mass balance condition greatly.

A considerable simplification is achieved by adopting the so-called bifurcation model. The model is based on the assumption that the multipcomponent diffusion coefficient between species i and j can be approximated by

$$D_{i,j} \approx \frac{\bar{D}}{F_i F_j}, \quad (44)$$

Here, \bar{D} is a reference diffusion coefficient, which is chosen in Ref. 14 to be the self diffusion coefficient of N_2 . Eq. (44) is theoretically rigorous if the interaction among species is purely by the induced dipole-induced dipole interactions. At temperatures of up to about 3000 K in air, molecular potentials are indeed almost those of induced dipole-induced dipole interactions. At higher temperatures, that is not so, and so a very rough approximation must be made with $D_{i,j}$'s in order to satisfy this condition. The values of F_i 's so selected are given in Ref. 14. F_s is proportional approximately to the square-root of its molecular weight relative to the reference species (which is 0.028 kg/mol for N_2):

$$F_s \approx \sqrt{\frac{M_s}{0.028}}. \quad (45)$$

If Eq. (44) holds, the bifurcation model states that the rate of mass diffusion of species s can be written as

$$J_s = \frac{\rho \bar{D} \mu_2}{M \mu_1} \frac{\partial Z_s}{\partial y} \quad \text{kg}/(\text{m}^2 - \text{s}), \quad (46)$$

where Z_s is a virtual mass fraction

$$Z_s = \frac{M_s X_s}{F_s \mu_1}, \quad (47)$$

and

$$\mu_1 = \sum_s X_s F_s, \quad \mu_2 = \sum_s \frac{M_s X_s}{F_s}. \quad (48a, b)$$

\bar{M} is the average molecular weight

$$\bar{M} = \sum_s X_s M_s.$$

The rate of production of species s by chemical reaction will be denoted by W_s . The conservation equation for species s can be written as

$$\rho u \frac{\partial \alpha_s}{\partial x} + \rho v \frac{\partial \alpha_s}{\partial y} = \frac{\partial}{\partial y} \left(\frac{\rho \bar{D} \mu_2}{\bar{M} \mu_1} \frac{\partial Z_s}{\partial y} \right) + \rho W_s. \quad (49)$$

The quantity $\bar{D} \mu_2 / (\bar{M} \mu_1)$ can be considered to be an effective diffusion coefficient:

$$D = \frac{\bar{D} \mu_2}{\bar{M} \mu_1}. \quad (50)$$

Schmidt number can now be defined as

$$Sc = \mu / \rho D. \quad (51)$$

Sc is a function of temperature, but is not a function of species. The virtual mass fraction Z_s in Eq. (47) can be written further as

$$Z_s = \frac{M_s X_s}{\sum_k M_k X_k} \frac{\sum_k M_k X_k}{F_s \mu_2} = \alpha_s \frac{\sum_k M_k X_k}{F_s \mu_2} = \alpha_s \frac{\bar{M}}{F_s \mu_2}$$

One can introduce a parameter C_s :

$$C_s = \frac{\bar{M}}{F_s \mu_2}. \quad (52)$$

Using these notations, the species conservation equation, Eq. (49), can be written as

$$\rho u \frac{\partial \alpha_s}{\partial x} + \rho v \frac{\partial \alpha_s}{\partial y} = \frac{\partial}{\partial y} \left[\frac{\mu}{Sc} \frac{\partial (C_s \alpha_s)}{\partial y} \right] + \rho W_s. \quad (53)$$

3.2. MASS BALANCE

In order to describe the behavior of an ablating wall, what happens inside the heatshield material, i.e., material response, needs to be calculated. This can be done by using a computer code such as Super Charring Materials Ablation (SCMA) code given in Ref. 15. The calculation will yield the mass flow rate of the pyrolysis gas issuing from the wall, \dot{m}_p . By invoking equilibrium among the various species constituting the pyrolysis gas, one can determine the mass flow rates of each of the species $\dot{m}_{p,s}$. The mass fraction of species s in the pyrolysis gas will be represented by $\alpha_{s,p}$.

The total mass flow rate emerging from the wall is the sum of the pyrolysis mass flow rate \dot{m}_p and the mass flow rate produced at wall \dot{m}_t

$$\rho_w v_w = \dot{m}_p + \dot{m}_t, \quad (54)$$

The surface mass removal rate \dot{m}_t is

$$\dot{m}_t = \text{sum of mass removal rates by surface reaction} \\ + \text{sum of mass removal rates by sublimation}$$

As can be seen from Eqs. (24) and (27), mass removal rates by surface reactions consist of terms proportional to $\alpha_{s,w}$. As can be seen from Eq. (17), the mass removal rates by sublimation consist of terms proportional to $\alpha_{s,w}$ and terms independent of $\alpha_{s,w}$. Thus, one can write

$$\dot{m}_t = \sum_s (\delta_s \alpha_{s,w} + \epsilon_s). \quad (55)$$

The parameters δ_s and ϵ_s are determined by adding up contributions from all surface chemical and

sublimation processes. For instance, sublimation into C_3 , Eq. (18), contributes

$$\begin{aligned}\delta_{C_3} &= -0.25\eta_{v,C_3}\rho_w C_{w,C_3}, \\ \epsilon_{C_3} &= \eta_{v,C_3}m_{C_3}n_{E,C_3}C_{w,C_3}.\end{aligned}$$

For a species s , the total mass flow rate at wall is the sum of the mass flow rate in the pyrolysis gas and the mass flow rate due to surface removal

$$\text{Species flow rate at wall} = \dot{m}_{p,s} + \dot{m}_{t,s}. \quad (56)$$

In the gas phase, at an infinitesimally small distance away from the wall, the species mass flow rate is the sum of a convective term, $\rho_w v_w \alpha_{s,w}$, and a diffusion term

$$\begin{aligned}\text{Species flow rate in gas phase} &= \rho_w v_w \alpha_{s,w} - \left(\frac{\rho \bar{D} \mu_2}{M \mu_1}\right)_w \left(\frac{\partial Z_s}{\partial y}\right)_w \\ &= \rho_w v_w \alpha_{s,w} - \frac{\mu}{Sc} \left[\alpha_{s,w} \left(\frac{\partial C_s}{\partial y}\right)_w + C_{s,w} \left(\frac{\partial \alpha_s}{\partial y}\right)_w\right].\end{aligned} \quad (57)$$

Because expression (56) and expression (57) must be equal to each other, one has

$$\dot{m}_{p,s} + \dot{m}_{t,s} = \rho_w v_w \alpha_{s,w} - \frac{\mu}{Sc} \left[\alpha_{s,w} \left(\frac{\partial C_s}{\partial y}\right)_w + C_{s,w} \left(\frac{\partial \alpha_s}{\partial y}\right)_w\right]. \quad (58)$$

On the other hand $\dot{m}_{t,s}$ can be written as

$$\dot{m}_{t,s} = \sum_k \gamma_{k,s} \alpha_{k,w} + \dot{m}_{v,s}. \quad (59)$$

For example, $\gamma_{k,s}$ by $O + C(c) \rightarrow CO$ is

$$\gamma_{O,O} = -0.25\eta_{r,O}\rho_w C_{w,O}.$$

The mass flow $\rho_w v_w$ can be written in turn as

$$\rho_w v_w = \dot{m}_p + \sum_s (\delta_s \alpha_{s,w} + \epsilon_s). \quad (60)$$

By substituting these into Eq. (58), one obtains the equation governing the wall value of mass fractions of species s as

$$\begin{aligned}\left[-(\dot{m}_p + \sum_k (\delta_k \alpha_{k,w} + \epsilon_k)) + \frac{\mu_w}{Sc_w} \left(\frac{\partial C_s}{\partial y}\right)_w\right] \alpha_{s,w} + \sum_k \gamma_{k,s} \alpha_{k,w} \\ + \frac{\mu_w}{Sc_w} C_{k,w} \left(\frac{\partial \alpha_s}{\partial y}\right)_w = -\dot{m}_{p,s} - \dot{m}_{v,s}.\end{aligned} \quad (61)$$

Eq. (61) forms a system of N simultaneous quadratic equations in $\alpha_{s,w}$'s. To determine α_w 's using this equation, one must determine the wall slope $(\partial \alpha_s / \partial y)_w$. The wall slope is determined by solving the flow field. Flow field can be solved for this purpose either by using the so-called two-layer method, i.e., inviscid layer plus boundary layer, or by using computational-fluid-dynamics (CFD). In the following, these two methods are reviewed.

3.3. APPLICATION TO BOUNDARY LAYER ANALYSIS

In the two-layer method, the inviscid flow field is solved by any available method. Then the boundary layer is attached to the inner boundary of the inviscid solution. The outer boundary condition of the boundary layer is thus given by the inner boundary value of the inviscid solution. It is believed that several computer codes exist in the world presently in which this method is used. To

a high accuracy, chemical equilibrium can be assumed at the edge of the boundary layer. However, within the boundary layer, frozen flow assumption is valid to a quite high accuracy.

Boundary layer analysis was introduced in Section 2.8. Here, we have to generalize it into off-stagnation points and to the case of Prandtl number different from 1, and, above all, must use the bifurcation model introduced above. Coordinate transformation is unchanged. The resulting differential equation becomes, for mass and momentum,

$$\left(\frac{\rho\mu}{\rho_e\mu_e}f''\right)' + ff'' + 2\beta\left(\frac{\rho_e}{\rho} - f'^2\right) = 2\xi\left(f'\frac{\partial f'}{\partial\xi} - \frac{\partial f}{\partial\xi}f''\right) \quad (62)$$

where

$$\beta = \frac{d[\ln(u_e)]}{d[\ln(\xi)]}.$$

The energy equation becomes

$$\left(\frac{\rho\mu}{\rho_e\mu_e}\frac{1}{Pr}g'\right)' + fg' + \frac{u_e^2}{H_e}\left[\left(1 - \frac{1}{Pr}\right)\frac{\rho\mu}{\rho_e\mu_e}f'f''\right]' = 2\xi\left(f'\frac{\partial g}{\partial\xi} - \frac{\partial f}{\partial\xi}g'\right). \quad (63)$$

The species equation is transformed into

$$\begin{aligned} \left(\frac{\rho\mu}{\rho_e\mu_e}\frac{C_s}{Sc}\alpha'_s\right)' + \left(f + \frac{\rho\mu}{\rho_e\mu_e}\frac{C'_s}{Sc}\right)\alpha'_s + \left[\left(\frac{\rho\mu}{\rho_e\mu_e}\frac{C'_s}{Sc}\right)' - 2f'\beta_s\right]\alpha_s \\ = 2\xi\left(f'\frac{\partial\alpha_s}{\partial\xi} - \frac{\partial f}{\partial\xi}\alpha'_s\right) \end{aligned} \quad (64)$$

where

$$\beta_s = \frac{d[\ln(\alpha_{s,e})]}{d[\ln(\xi)]}.$$

There are N (number of species) equations of the form Eq. (64).

Eqs. (62) to (64) form a system of nonlinear ordinary differential equations because a) Eq. (62) contains terms consisting of products of dependent variables, and (b) ρ_e/ρ in Eq. (62) depends nonlinearly on g and α 's. This system of equations can be solved through approximate linearization and iteration. In the end, at each ξ -point, the solution of the species equations can be written as

$$\alpha_s(\eta) = \alpha_{s,w}Y_1(\eta) + \alpha'_{s,w}Y_2(\eta) + Y_p(\eta). \quad (65)$$

where the homogeneous solutions Y_1, Y_2 and the particular solution Y_p are chosen so that

$$Y_1(0) = 1, \quad Y'_1(0) = 0,$$

$$Y_2(0) = 0, \quad Y'_2(0) = 1,$$

$$Y_p(0) = 0, \quad Y'_p(0) = 0.$$

By demanding that α_s value in Eq. (65) becomes the boundary layer edge value at the boundary layer edge, one has

$$\alpha_{s,w}Y_1(s, \eta_e) + \alpha'_{s,w}Y_2(s, \eta_e) + Y_p(s, \eta_e) = \alpha_{s,e}. \quad (66)$$

There are N equations of the form (66).

Eq. (61) is converted into the boundary layer coordinates by introducing

$$\frac{\partial\alpha_s}{\partial y} = \frac{d\eta}{dy}\alpha'_s$$

which leads to a system of simultaneous nonlinear algebraic equations:

$$\begin{aligned} [-\dot{m}_p + \sum_k(\delta_k\alpha_{k,w} + \epsilon_k) + \frac{\mu_w}{Sc_w}\left(\frac{\partial\eta}{\partial y}\right)_w C'_{s,w}]\alpha_{s,w} + \sum_k\gamma_{k,s}\alpha_{k,w} \\ + \frac{\mu_w}{Sc_w}C_{k,w}\left(\frac{\partial\eta}{\partial y}\right)_w\alpha'_{s,w} = -\dot{m}_{p,s} - \dot{m}_{v,s}. \end{aligned} \quad (67)$$

Eqs. (66) and (67) form $2N$ algebraic equations containing $2N$ unknowns $\alpha_{s,w}$ and $\alpha'_{s,w}$. These equations can be solved through approximate linearization and iteration. The values of $\alpha_{s,w}$ are first assumed. These values are used in evaluating $\delta_k \alpha_{k,w}$. Then there results a system of linear equations of order $2N$

$$[A]X = R.$$

Here,

$$\begin{aligned} \text{For } k = 1 \text{ to } N : X &= \alpha_{k,w}, \\ \text{For } k = N + 1 \text{ to } 2N : X &= \alpha'_{k,w}. \end{aligned}$$

This equation set is solved as

$$X = [A]^{-1}R,$$

to obtain improved values of $\alpha_{s,w}$ and $\alpha'_{s,w}$. For the next iteration,

$$\text{Next } \alpha_{s,w} = \epsilon \times (\text{New } \alpha_{s,w}) + (1 - \epsilon) \times (\text{old } \alpha_{s,w}) \quad (68)$$

where ϵ is a number smaller than 1, is used in the evaluation of $\delta_k \alpha_{k,w}$, and so forth. This process is repeated until a converged set of solution vector is obtained. Experience has shown that the most appropriate value of ϵ varies between 0.2 and 1 depending on the problem.

3.4. APPLICATION TO CFD

CFD codes are believed to exist worldwide in which the kinetic boundary conditions are applied as outlined in this lecture (e.g. Ref. 16). In CFD, the relation (61) becomes the boundary condition for species variables. The wall slope $(\partial \alpha_s / \partial y)_w$ is written in a difference form. Because Eq. (61) is nonlinear in $\alpha_{s,w}$, approximate linearization must be carried out. It can be achieved by assuming $\delta_k \alpha_{k,w}$ to be known. In updating $\delta_k \alpha_{k,w}$, it would be wise to correct only partly, i.e. use Eq. (68), to ensure stability.

Applying the boundary condition of a linear form will not be of any difficulty in the CFD community. If a two-point representation of wall slope is used, Eq. (61) will supply the diagonal term and one off-diagonal term in the difference formulation. If a three-point representation of wall slope is used, two off-diagonal terms will be specified. If a steady-state solution is sought and if the solution is obtained by a time-asymptotic method, the approximate linearization scheme will be implemented by updating $\delta_k \alpha_{k,w}$ after each iteration. If a time-accurate solution is sought, a unique iterative procedure must be devised in which the iteration is performed while time is frozen.

4.0. SURFACE PROBLEMS IN PLANETS

4.1. EARTH ENTRIES

In Earth's atmosphere, the gas-surface interaction problem was studied in the past mostly in two areas: catalytic recombination of oxygen and ablation of carbonaceous heatshield. Goulard's pioneering work for the stagnation point was discussed already. His work was extended to off-stagnation points, three dimensional flows, and to nitrogen recombination by various researchers.

Until recently, ablation phenomenon was treated by invoking gas-surface equilibrium. The assumption of gas-surface equilibrium circumvents the need to know the $\eta_{r,f}$ and $\eta_{v,f}$. In the kinetic approach, the equilibrium condition can be reached by assuming $\eta_{r,f}$ and $\eta_{v,f}$ to be a large number. According to Eqs. (8a), $\eta_{r,f}$ and $\eta_{v,f}$ need only to be much larger than $M_w / \sqrt{Re_\infty}$ to produce an effect of a gas-surface equilibrium. The equilibrium approach and the kinetic approach have been compared in Ref. 13. It found that equilibrium approach gives always higher ablation rate than the kinetic approach.

The recent data on nitridation¹⁰, $N + C(c) \rightarrow CN$, which gives $\eta_{r,f}$ to be 0.3, has brought an alarm and skepticism of the measurement¹³. This is because, if the measured value of $\eta_{r,f}$ is accurate, this process will be the major process of ablation in a hyperbolic Earth entry. More experiment is desirable.

For wall heat transfer rates in the range from 5×10^5 and 1.5×10^6 W/m², such as in the stagnation region of the nose cone of the Space Shuttle, carbon-carbon composite overcoated with silicon carbide,

SiC, is used for the surface. When exposed to a stream containing atomic oxygen, SiC is converted quickly to SiO₂. SiO₂ is in an amorphous form. Oxygen atoms are dissolved in this amorphous SiO₂, diffuse, and reach the SiC substrate. Once they reach the SiC substrate, they combine with C to form gaseous CO. These CO molecules are dissolved in SiO₂, diffuse, and escape from the surface, leaving SiO₂. This phenomenon has been studied experimentally to a considerable extent in Europe and in Japan. Yet, there are no theoretical model to describe the rate process quantitatively.

In the future, attempts will be made to construct an airbreathing hypersonic vehicle. High heating rates will occur at the nose tip, wing leading edge, cowl lip, and in the combustion chamber of such a vehicle. New material such as hafnium di-boride, HfB₂, may be used for such high heating areas. Gas-surface interaction for such a new material will be a challenge.

The ablation rate of carbonaceous heatshield material in the nose region of a blunt body was measured systematically in Ref. 17. The measured ablation rate was about 3 times higher than calculated assuming gas-surface equilibrium in the stagnation region. This cannot be attributed to roughness-caused turbulence because surface roughness cannot produce turbulence at the stagnation point, because velocity is zero there. In Ref. 18, this large ablation rate is attributed to the turbulence generated by ablation.

Various experiments showed that the highest heating rates occur at points away from the stagnation point, somewhere where the surface normal is about 40° with respect to the flow direction (see, e.g, Ref. 19). This peak-heating region is usually the point where turbulent transition occurs due to roughness. In many cases it coincides also with the point of sphere-cone juncture where an adverse pressure gradient occurs. Heat transfer rate in the region downstream of this point is usually higher than the heat transfer rate to the stagnation point, and therefore the ablation rate is also higher there. Theoretical prediction of the ablation rate in this downstream region from the first principles is at this time not yet achieved. To do so, one needs to correctly model injection-induced turbulence and roughness-induced turbulence.

If one can model turbulence accounting for these effects, then the theory given in Chapter 3 can be applied. The only part that needs modification is viscosity μ which will have to be modified to include the effect of turbulence.

Because there is a large uncertainty about the behavior of turbulence in the downstream region, the heatshield is usually over-designed. In the past, this philosophy was proven to be effective and necessary.

4.2. MARTIAN ENTRIES

Martian entries occur typically at 6 km/s. The density of the atmosphere is about 1/70 of that of the Earth. Heating rate does not exceed 4×10^6 W/m². A material made of silica matrix impregnated with an organic resin is used as an ablating heatshield. As mentioned earlier, Martian atmosphere consists mostly of CO₂. At the edge of boundary layer, CO₂ is dissociated into CO and O. CO and O diffuse through the boundary layer and reach the wall. At wall, CO + O → CO₂ can conceivably occur. The surface of the material during entry is pure silica. As mentioned, silica shows a near-zero reaction coefficient for CO + O.

One uncertainty is about the effect of surface roughness on the effective recombination coefficient, Eq. (21). Because we do not know the BET area of a Martian heatshield during an entry flight, we cannot determine the effective recombination coefficient. In addition, we do not know where turbulent transition occurs because we do not know the intensity of the injection-induced turbulence or the roughness-induced turbulence.

4.3. VENUSIAN ENTRIES

The atmospheric composition of the planet Venus is similar to that of Mars. But the density of the atmosphere is about 70 times that of the Earth, and the entry speed is more than 10 km/s. At the peak-heating point, the pressure at the stagnation point is of the order of 10 atm. The combination of the density and entry speed produces heating rates in the range of several million W/m². Only carbonaceous ablation material can be used as heatshield. The comments about carbon surface made in Chapters 1 and 2 are applicable.

In the Pioneer-Venus Probe mission, four probe vehicles entered into the Venusian atmosphere. Each vehicles were equipped with two thermocouples in their heatshield, one near the stagnation

point and the other near the frustum edge. The data from these thermocouples indicated that the heat transfer rates were higher at the frustum edge than at the stagnation point. The flight data are consistent with the assumption of a turbulent flow.^{20,21}

In this entry flights, the edge of boundary layer will contain oxygen atoms and a small concentration of nitrogen atoms. The reactions (13) and (14) will occur. Reaction (13) will contribute considerably to the total heat transfer rate. Sublimation reaction (18) will occur also.

4.4. TITAN ENTRIES

The atmosphere of Titan consists mostly of N_2 , with a small amount of CH_4 . The density of the atmosphere is nearly the same as that of the Earth. For the Huygens vehicle sent by the European Space Agency, the entry velocity was about 5 km/s. However, in future missions, entry velocity of up to about 14 km is possible. Radiation from the CN becomes a major component of heat transfer rate. Both a silica-based and a carbon-based heatshield can be used for these entries. There will be a small amount of dissociation of N_2 , and full dissociation of CH_4 . Reactions (15) and (16) will occur in both directions.

4.5. OUTER PLANET ENTRIES

Atmosphere of the outer planets consists of hydrogen and helium. Entry into Jupiter has been made in the Galileo Probe mission. Heat transfer was due overwhelmingly by radiation. The heatshield was made with a carbon-based material. During this entry flight, progression of surface recession was measured. The flight data showed a surprisingly low surface recession at the stagnation region and surprisingly high recession at the frustum.

The low recession in the stagnation region is attributed to thermal nonequilibrium.²² The high recession in the frustum region is attributed to increase in radiation due to turbulence caused by ablation.²³ The dominant gas-surface interaction was sublimation, reaction (18). The sublimation rate was driven essentially by the energy conservation law, rather than by surface kinetics.

In a futuristic mission, one can conceive entry flights into Saturn, Uranus, or Neptune. In such entries, radiative heating will be much less than that to the Galileo Probe. There, not only the sublimation but the reactions, Eqs. (15) and (16) could conceivably become important. Surface kinetics may play a role.

5.0. CONCLUDING REMARKS

In the above, gas-surface interaction problem was studied from the kinetic approach. The kinetic approach enables rational way of quantitatively evaluating the surface phenomena in determining heat transfer rates and surface ablation rates. The study identifies areas of uncertainty also, which are: 1) the effective coefficients of gas-surface interactions for rough surfaces, and 2) the intensity of turbulence for a rough surface in the presence of ablation. As a minor and overcomable difficulty, nonlinearity in the governing equations at wall is pointed out.

The problem of gas-surface interaction in hypersonic flight contains several different disciplines that are tied together in a rather unexpected way. Because of the unusual nature of the problem, the traditional discipline-based approach to the problem becomes difficult to apply. This is probably the reason for the misunderstanding and mismanagement of the issues that existed in the past. To ensure mission success in the midst of such uncertainties, the planetary entry vehicles had been designed in the past with a rather large safety factor. In retrospect, we feel that such large safety factors were justified, because several unexpected phenomena occurred. For a rational management of the future space programs, all scientific issues about gas-surface interaction will have to be understood better by all involved. Much more research on the subject is highly desirable.

6.0. REFERENCES

- [1] Goulard, R. (1958). *Catalytic Recombination Rates in Hypersonic Stagnation Heat Transfer*. Jet Propulsion, Vol. 28, No. 11, pp. 737-745.
- [2] Winkler, E. L., & Sheldahl, R. E. (1966). *Influence of Calorimeter Surface Treatment on Heat-Transfer Measurements in Arc-Heated Test Streams*. AIAA Journal, Vol. 4, No. 4, pp. 715-716.

- [3] Park, C., Raiche, G. A., II, Driver, D. M., Olejniczak, J., Terrazas-Salinas, I., Hightower, T. M. & Sakai, T. (2004). *Comparison of Enthalpy Determination Methods for an Arc-jet Facility*. AIAA Paper 2004-0487, January 2004.
- [4] Liu, G. N-K. (1973). *High Temperature Oxidation of Graphite by a Dissociated Oxygen Beam*. Ph.D thesis, Massachusetts Institute of Technology, Department of Aeronautics and Astronautics.
- [5] Sepka, S., Copeland, R. A., Marshall, J., & Chen, Y-K. (1999). *Experimental Investigation of Surface Reactions in Carbon Monoxide and Oxygen Mixtures*. AIAA Paper 99-3629.
- [6] Pagni, P. J. (1972). *Comparison of Diffusion Theory Adsorption and Desorption Rates with Experimental Lifetimes*. University of California College of Engineering Report No. ME-72-9.
- [7] Somorjai, G. A. (1972). *Principles of Surface Chemistry*. Prentice-Hall, Engldwood Cliffs, NJ., pp. 209-213.
- [8] Somorjai, G. A. (1972). *Principles of Surface Chemistry*. Prentice-Hall, Engldwood Cliffs, NJ., p. 245.
- [9] Park, C. (1990). *Nonequilibrium Hypersonic Aerothermodynamics*. John Wiley, p 351.
- [10] Park, C. & Bogdanoff, D. W. (2003). *Shock Tube Measurement of Coefficient of Reaction of Nitrogen Atoms with Solid Carbon: Preliminary Results*. AIAA Paper 2003-0158.
- [11] Chase, M. W., Davies, C. A., Downey, J. R., Jr., Frurip, D. J., McDonald, R. A., & Syverud, A. N. (1985). *JANAF Thermochemical Tables, Part 1. Al-Co, Part 2. Cr-Zr*. American Chemical Society.
- [12] Baker, R. L., McDonough, J. M., Herr, K. C., Klingberg, R. A., Coffey, J. C., & Covington, M. A. (1984). *Carbon Vaporization and Condensation Effects*. NASA TM 874300.
- [13] Chen, Y. K. & Milos, F. S. (2004). *Finite-Rate Ablation Boundary Conditions for a Carbon-Phenolic Heat-Shield*, AIAA Paper 2004-2270.
- [14] Park, C., Jaffe, R. L., & Partridge, H. (2001). *Chemical-Kinetic Parameters of Hyperbolic Earth Entry*. Journal of Thermophysics and Heat Transfer, Vol. 15, No. 1, pp. 76-90.
- [15] Ahn, H. K., Park, C., & Sawada, K. (2002). *Response of Heatshield Material at Stagnation Point of Pioneer-Venus Probes*. Journal of Thermophysics and Heat Transfer, Vol. 16, No. 3, pp. 432-439.
- [16] Park, C. (2004). *Stagnation-Point Radiation for Apollo 4*. Journal of Thermophysics and Heat Transfer, Vol. 18, No. 3, pp. 349-357.
- [17] Wool, M. R. (1975). *Final Summary Report Passive Nosedip Technology (PANT) Program*. SAMSO-TR-75-250.
- [18] Park, C. (1984). *Injection-Induced Turbulence in Stagnation-Point Boundary Layers* AIAA Journal, Vol. 22, No. 2, pp.219-225.
- [19] Park, C. & Balakrishnan, A. (1985). *Ablation of Galileo Probe Heat-Shield Models in a Ballistic Range*. AIAA Journal, Vol. 23, No. 2, pp.301-308.
- [20] Ahn, H. K., Park, C., & Sawada, K. (2002). *Response of Heatshield Material at Stagnation Point of Pioneer-Venus Probes*. Journal of Thermophysics and Heat Transfer, Vol. 16, No. 3, pp. 432-439.
- [21] Takahashi, M. & Sawada, K. (2002). *Simulation of Entry Flight Flowfield over Four Probe Vehicles in Pioneer-Venus Mission*. AIAA Paper 2002-0909.
- [22] Park, C. (2005). *Overview of Radiation Problems in Planetary Entries*. Proceedings of the International Workshop on Radiation of High Temperature Gases in Atmospheric Entry - Part 2, European Space Agency SP 583, pp. 3-14.
- [23] Matsuyama, S., Shimogonya, Y., Ohnishi, N., Sawada, K. & Sasoh, A (2002) *Numerical Simulation of Galileo Proe Entry Flowfield with Radiation*. AIAA Paper 2002-2994.